

Atmospheric Response to Modified CLIMAP Ocean Boundary Conditions during the Last Glacial Maximum*

E. RICHARD TORACINTA

Polar Meteorology Group, Byrd Polar Research Center, The Ohio State University, Columbus, Ohio

ROBERT J. OGLESBY

NASA Marshall Space Flight Center/National Space Science and Technology Center, Huntsville, Alabama

DAVID H. BROMWICH

Polar Meteorology Group, Byrd Polar Research Center, and Atmospheric Sciences Program, Department of Geography, The Ohio State University, Columbus, Ohio

(Manuscript received 4 December 2002, in final form 2 July 2003)

ABSTRACT

Global climate simulations are conducted to examine the sensitivity of the Last Glacial Maximum (LGM) climate to prescribed sea surface temperatures (SSTs) that are modified from the Climate: Long-range Investigation, Mapping, and Prediction (CLIMAP) study. Based on the consensus from various LGM proxy data, the SSTs are cooled by 4°C uniformly in the Tropics (30°N–30°S) relative to CLIMAP, and the high-latitude sea ice extent is reduced. Compared to results from a simulation with CLIMAP SSTs, the modified LGM SSTs cause significant opposing changes in the hemispheric and regional-scale atmospheric circulation, which are most pronounced in the winter hemisphere. For instance, there is significant weakening of the midlatitude circulation and reduction of 500-hPa eddy kinetic energy and midlatitude precipitation resulting from the decreased meridional temperature gradient in the modified SST simulation. In contrast, reduced sea ice extent during the boreal winter causes increased regional baroclinicity and intensified atmospheric circulation in the western North Pacific and the North Atlantic. Cooled tropical SSTs also increase the land–ocean temperature contrast, which strengthens the Asian summer monsoon circulation. Both LGM simulations produce enhanced low-level convergence and increased precipitation along the South Pacific convergence zone (SPCZ) relative to present day, despite the cooler LGM climate. The SPCZ orientation and intensity are closely linked to the distribution of South Pacific SSTs. Comparison of surface temperature estimates from land- and ocean-based proxy data with model output suggests that uniform cooling of the tropical SSTs and modification of the high-latitude sea ice extent may be sufficient to accurately simulate the first-order characteristics of the LGM climate.

1. Introduction

Sea surface temperatures (SSTs) are an important component of the global climate system. At low latitudes, SSTs are closely tied to the distribution of atmospheric deep convection, which in turn drives large-scale atmospheric circulation via latent heat release (Webster 1972; Graham and Barnett 1987; Lindzen and Nigam 1987; Zhang 1993). Large-scale SST anomalies in the equatorial Tropics have a first-order impact on atmospheric standing wave patterns and climate con-

ditions globally (e.g., the contemporary El Niño–Southern Oscillation; Horel and Wallace 1981; Cane 1983; Rasmusson and Wallace 1983). At high latitudes, SSTs influence the concentration and extent of sea ice, which modulates the surface energy balance with direct implications for air–sea interactions and atmospheric circulation.

Although sea surface temperatures represent a critical lower boundary condition for global-scale paleoclimate simulations, the magnitude and distribution of SSTs at the Last Glacial Maximum (LGM), roughly 21 000 calendar years before present (21 kyr B.P.; Mix et al. 2001), remain uncertain. Climate: Long-range Investigation, Mapping, and Prediction (CLIMAP; CLIMAP 1981) produced the first systematic, global reconstruction of LGM SSTs by relating the distribution of various plankton species in marine sediment cores to the temperature of the near-surface waters they inhabit. Relative to the

* Byrd Polar Research Center Contribution Number 1273.

Corresponding author address: Dr. E. Richard Toracinta, Byrd Polar Research Center, The Ohio State University, 1090 Carmack Road, Columbus, OH 43210-1002.
E-mail: toracint@polarmet1.mps.ohio-state.edu

present, the CLIMAP reconstruction shows annual mean (average of February and August estimates) cooling of less than 2°C throughout much of the equatorial Tropics. Roughly the same magnitude of warming is predicted in the subtropical Pacific Ocean gyres where only a few core samples were available. Early global climate model (GCM) simulations of the LGM climate using the CLIMAP SSTs failed, however, to produce the magnitude of atmospheric cooling or change in the hydrologic cycle at low latitudes suggested by some terrestrial evidence. For instance, Rind and Peteet (1985) report little change in simulated LGM precipitation at low latitudes relative to today, whereas proxy data (e.g., fossil dunes) indicate widespread aridity in the LGM Tropics.

Land and ocean-based proxy methods for reconstructing low-latitude surface temperatures at the LGM are varied. Over the oceans, LGM SST estimates are typically based on the analysis of the compositions of planktonic species, changes in their stable isotopes, the organic compounds (long-chain alkenones) produced by plankton, or a combination of methods (multiproxy approach). For instance, Trend-Staid and Prell (2002) examined planktonic foraminiferal samples from the Atlantic, Pacific, and Indian Ocean basins using the modern analog technique (Prell 1985), by which statistical measures of dissimilarity are applied to a large number of core-top (i.e., modern) samples to select species compositions that most resemble those from the LGM. The modern SSTs for the selected modern analog samples are then averaged to derive glacial SSTs. The Trend-Staid and Prell (2002) LGM annual mean SST estimates show little cooling relative to present, particularly in the western tropical Pacific and Indian Oceans (similar to CLIMAP), but substantial cooling (2°–8°C) in the eastern tropical Atlantic and Pacific. Lee et al. (2001) applied the modern analog technique to plankton assemblages from sediment cores near Hawaii. Their analysis indicates a 2°C cooling of the annual mean LGM SSTs in the subtropical North Pacific rather than the 1°–2°C warming suggested by CLIMAP.

A number of alkenone-based point estimates of LGM SSTs are generally consistent with the CLIMAP reconstruction showing relatively little change (<2°C) relative to present in the Tropics (e.g., Bard et al. 1997; Lyle et al. 1992; Ohkouchi et al. 1994; Sikes and Keigwin 1994; Sonzogni et al. 1998). SST estimates derived from radiolarian microfossils assemblages in equatorial eastern Pacific sediments indicate a 4°C cooling relative to present (Pisias et al. 1997; Pisias and Mix 1997), whereas analysis of the magnesium content in planktonic forams suggests that LGM SSTs in the equatorial Atlantic and Pacific basins were generally 2.5°–3°C cooler than today (Hastings et al. 1998; Lea et al. 2000). Guilderson et al. (1994) suggests a much greater SST cooling (5°C) in the Caribbean based on the ratio of strontium to calcium in corals, which has been found to vary with water temperature (Beck et al. 1992). This estimate of cooling has been challenged by Crowley

(2000) who questions whether ice age corals could have survived in tropical waters that were 5°C cooler than present.

In contrast to the broad consensus from ocean-based paleothermometry of modest tropical SST cooling at the LGM, a variety of land-based proxy sources provide evidence of substantial low-latitude cooling. For instance, by exploiting the temperature dependence of noble gas solubility, terrestrial surface temperature estimates for the LGM have been derived from the concentrations of noble gases in the groundwater taken from deep aquifers in Brazil and the southern United States (Stute et al. 1992; Stute et al. 1995a,b). Data from these sites indicate that mean annual surface temperatures during the LGM were approximately 5°C cooler than present. Colinvaux et al. (1996) reached a similar conclusion based on the presence of pollen varieties, from certain cold-adapted plant taxa, found in lake sediment cores in the Amazon lowlands. Rind and Peteet (1985) summarize the findings of several studies indicating snowline or vegetation zone depressions of about 1 km during the LGM at several tropical locations. Assuming a moist adiabatic atmospheric lapse rate, these changes correspond to a 5°–6°C cooling of the annual mean surface temperature at the LGM, consistent with other tropical land-based proxy estimates. However, Broccoli (2000) urges caution when interpreting these data since the temperature lapse rate along the surface slope may not be the same as the free atmospheric lapse rate.

Oxygen isotope variations in ice cores from tropical alpine glaciers are also being utilized as paleothermometers. Bradley et al. (2003) demonstrate that the relative abundance of ¹⁸O to ¹⁶O (i.e., δ¹⁸O) in cores from mountain glaciers in South America (Thompson et al. 1998) and the Tibetan Plateau (Thompson et al. 2000) are highly correlated with SSTs in the equatorial Pacific, which modulate the atmospheric circulation via deep convection. In turn, the circulation anomalies have a first-order impact on the temperature and precipitation anomalies at the ice core sites. The robust statistical relationships between tropical Pacific SSTs and ice core δ¹⁸O are achieved when the seasonality of accumulation is used to calibrate the isotopic records in the cores. Thus calibrated, the long-term isotopic record from the South American ice cores indicates that annual mean LGM SSTs in the central and eastern Pacific were approximately 3.5°C colder than today.

With regard to the reconstruction of ocean conditions at high latitudes, analyses of diatom assemblages in Southern Ocean sediment cores indicate a larger seasonal cycle of the circum-Antarctic sea ice extent during the LGM than predicted by CLIMAP. Recent estimates of the LGM summer sea ice margin in specific sectors of the Southern Ocean vary, however, from the location of the present-day winter extent (Gersonde and Zielinski 2000) to very near the present-day minimum (Crosta et al. 1998a,b). Coupled ocean–atmosphere model results (Manabe and Broccoli 1985; Weaver et al. 1998; Bush

and Philander 1999; Shin et al. 2003) also indicate a much larger seasonal cycle of the Antarctic sea ice than predicted by CLIMAP. These particular model simulations are not constrained by micropaleontological evidence of LGM sea ice conditions and some discrepancies between modeled sea ice extent and proxy-based reconstructions, particularly in data-sparse regions of the Southern Ocean, have yet to be resolved (Armand 2000; Hewitt et al. 2001b).

In the North Atlantic, the CLIMAP reconstruction shows permanent sea ice in the Greenland, Iceland, and Norwegian (GIN) Seas. This prediction is challenged, however, by a body of LGM SST estimates based on dinoflagellates (de Vernal and Hillaire-Marcel 2000), coccoliths (Hebbeln et al. 1994), biomarker pigments (Rosell-Melé and Koç 1997), alkenone abundance (Rosell-Melé and Comes 1999), and foraminifera (Weinelt et al. 1996; Veum et al. 1992) in marine sediment cores. These data indicate that portions of the North Atlantic were relatively warm with the GIN Seas at least seasonally ice free during the LGM. This prediction is corroborated by ocean surface circulation patterns inferred from foraminiferal assemblages in the northeast Atlantic (Lassen et al. 1999) and from coupled ocean-atmosphere model simulations (Hewitt et al. 2001a,b; Hewitt et al. 2003; Shin et al. 2003). Seasonally open water in the North Atlantic at the LGM has important implications for the mass balance of the Northern Hemisphere continental ice sheets (Ruddiman and McIntyre 1979; Hebbeln et al. 1994).

Proxy data provide a critical framework for improving the SST boundary conditions in numerical simulations of the LGM climate and various methodologies have been employed to modify the prescribed ocean boundary condition used in GCM simulations. Several previous studies have tested the climate response to either regional or large-scale changes in SST forcing and most focus primarily on the Northern Hemisphere where the climate response to LGM boundary conditions tends to be greatest (e.g., Marsiat and Valdes 2001). Rind and Peteet (1985) applied a uniform 2°C cooling to the global CLIMAP SST dataset. Their GCM simulations produced low-latitude conditions that matched closely the proxy data in most tropical locations. Mix et al. (1999) reconstructed SSTs in the tropical eastern Pacific and tropical Atlantic basins based on time-varying faunal assemblages from marine sediment cores. Their prediction differs markedly from CLIMAP in these regions with 3°–5°C cooling relative to present in the tropical eastern Pacific (perpetual La Niña) and 3°–6°C in the tropical Atlantic. Using this SST reconstruction, Hostetler and Mix (1999) obtained GCM results for the LGM in general agreement with terrestrial proxy data. However, their study focused on the tropical response to specific regional SST forcing and did not consider SST changes in other tropical basins (e.g., the western Pacific warm pool) or at high latitudes.

Yin and Battisti (2001) modeled the LGM climate

using prescribed SSTs that were 3°C cooler than CLIMAP in the global Tropics (14°N–14°S). They found that the large-scale atmospheric circulation changes at midlatitudes due to the imposed cooler tropical SSTs are small relative to the atmospheric response to altered SST gradients. Their study did not include the effect of modified high-latitude SSTs or sea ice. Charles et al. (2001) test the sensitivity of the simulated global hydrologic cycle and the resulting terrestrial $\delta^{18}\text{O}$ signature to cooled SSTs in the Tropics and subtropics. Similar to Yin and Battisti (2001), they note that large-scale atmospheric dynamics are most sensitive to tropical SST gradients.

This paper presents the results of three 15-yr GCM simulations of the present-day and LGM climate. The objective is to quantify the global and regional-scale atmospheric response to a prescribed ocean boundary condition that is modified relative to CLIMAP based on available terrestrial and ocean proxy data. Our approach is similar to that of Yin and Battisti (2001). However, unlike theirs and other modeling studies using prescribed SSTs, the present study examines the dynamic and thermodynamic response of the LGM atmosphere to improvements in the SST boundary conditions both in the Tropics and the Northern and Southern Hemisphere high latitudes. Section 2 describes the GCM and the boundary conditions used for each simulation. The results from a present-day control, a CLIMAP simulation, and an LGM simulation with modified SSTs are given in section 3 with discussion and conclusions in section 4.

2. Model and experiments

The National Center for Atmospheric Research (NCAR) Community Climate Model (CCM3; Kiehl et al. 1998) is a global spectral atmospheric model with T42 truncation (2.8° latitude \times 2.8° longitude transform grid), 18 hybrid sigma levels in the vertical, and a 20-min time step. The CCM3 includes a fully interactive Land Surface Model (LSM; Bonan 1998) to evaluate surface fluxes of heat, moisture, and momentum. The standard releases of CCM3 (version 3.6.16) and LSM (version 1) were used in the present study to simulate the present-day and LGM climates.

a. Model boundary conditions

Contemporary values for orbital forcing and trace gases (CO_2 , CH_4 , O_3 , and CFCs) were specified as boundary conditions in the present-day climate simulation, along with monthly mean climatological sea surface temperatures (Shea et al. 1992). The two LGM runs were given identical boundary conditions with the exception of the SSTs and sea ice extent. Elevation data for the Northern Hemisphere (Laurentide and Fennoscandian) ice sheets and Antarctic ice sheets were implemented from the University of Maine Ice Sheet Mod-

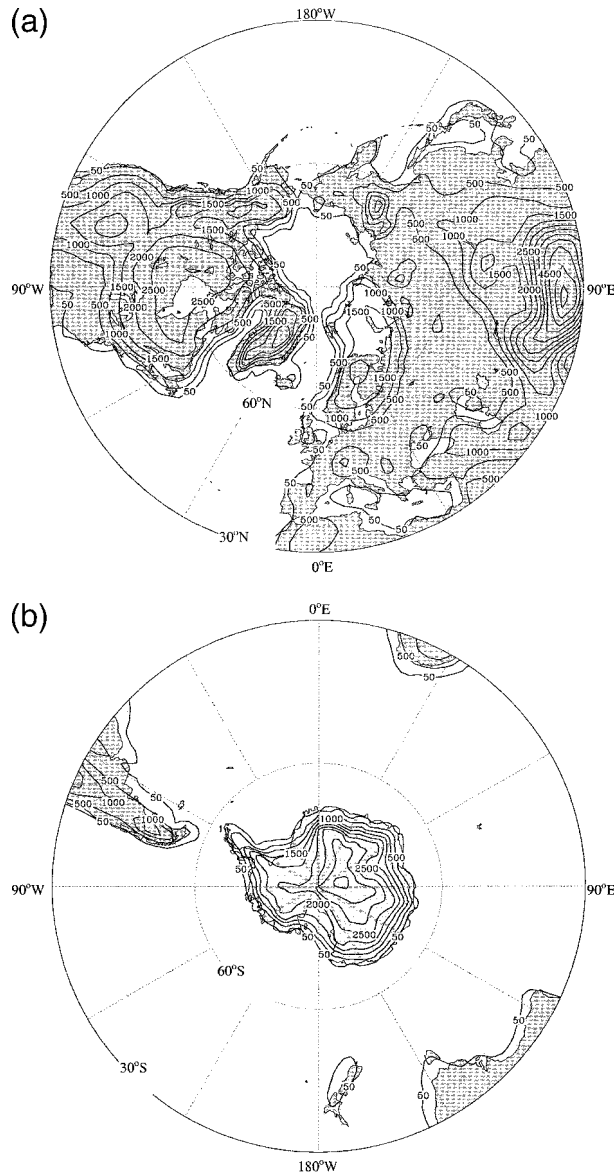


FIG. 1. (a) Northern Hemisphere terrain elevations for the CCM3 LGM simulations. Contour interval is 500 m. (b) The same as in (a) except for the Southern Hemisphere.

el output (UMISM; Fastook and Chapman 1989; Fastook and Prentice 1994). The UMISM is a time-dependent finite-element model that solves the mass continuity equation for ice flow and provides the ice surface elevation, isostatically adjusted bedrock elevation, column-integrated ice velocities, and internal temperatures within the ice column at each model grid point. The model also calculates creep deformation of the ice and includes a sliding mechanism at locations where the basal temperature reaches the pressure melting point. Surface accumulation rates are derived from a simple climatological model that provides accumulation and ablation rates dependent on the average annual temperature at the ice surface. The mass balance scheme,

TABLE 1. Orbital parameters for the LGM and present day (Berger 1978).

	LGM	Present day
Eccentricity	0.01899	0.01672
Obliquity	22.949°	23.446°
Lon of perihelion	114.42°	102.04°

originally derived for Antarctica (Fortuin and Oerlemans 1990; Fastook and Prentice 1994), arrives at an annual mean temperature based on the atmospheric lapse rate and latitudinal temperature gradient. From this temperature, a net accumulation rate is obtained for each model grid point based on the saturation vapor pressure and local surface slope. The net ablation rate is obtained by imposing a latitudinally modified seasonal amplitude onto the annual mean temperature and counting positive degree days.

Figure 1a shows the LGM Northern Hemisphere terrain elevations on the CCM3 grid. The maximum Laurentide Ice Sheet elevation is 3200 m (relative to present-day sea level) just west of Hudson Bay and the southern margin approaches 38°N. The Fennoscandian Ice Sheet, with maximum elevation of 2200 m, extends from western Scotland across Scandinavia to the Barents and Kara Seas. In the Southern Hemisphere (Fig. 1b), the most significant elevation changes over Antarctica during the LGM occur on the West Antarctic Ice Sheet where elevations are 500–1500 m greater than present across Marie Byrd Land. This additional LGM ice fills the embayments of the Ross and Weddell Seas and extends along the Antarctic Peninsula. Modeled terrain elevations across the East Antarctic Ice Sheet at the LGM are generally within 50 m of present-day values with little if any ice advance beyond the present-day margins. The modeled Antarctic LGM ice extent is consistent with a recent reconstruction by Anderson et al. (2002) based on marine geological evidence. Elevation data from the Patagonian ice cap in southern South America, which covered 1800 km along the crest of the Andes during the LGM (Hollin and Schilling 1981), were taken from glacial model output by Hulton et al. (2002).

Global sea level was lowered by 120 m commensurate with the LGM ice sheet volume from glaciological model output. This value is intermediate between the 105 m sea level lowering in the Peltier (1994) LGM topography reconstruction and larger estimates (~130 m) based on marine proxy evidence (e.g., Yokoyama et al. 2000). The orbital parameters were set to 21 kyr B.P. values (Berger 1978; Table 1) and the CO₂ and CH₄ concentrations were set to 180 ppm and 350 ppbv, respectively. Although global vegetation maps for the LGM are available (e.g., Crowley and Baum 1997), discrepancies between these reconstructions and site-based vegetation predictions from proxy data (Prentice et al. 2000) motivated the decision to prescribe modern vegetation in ice-free regions in each of our simulations.

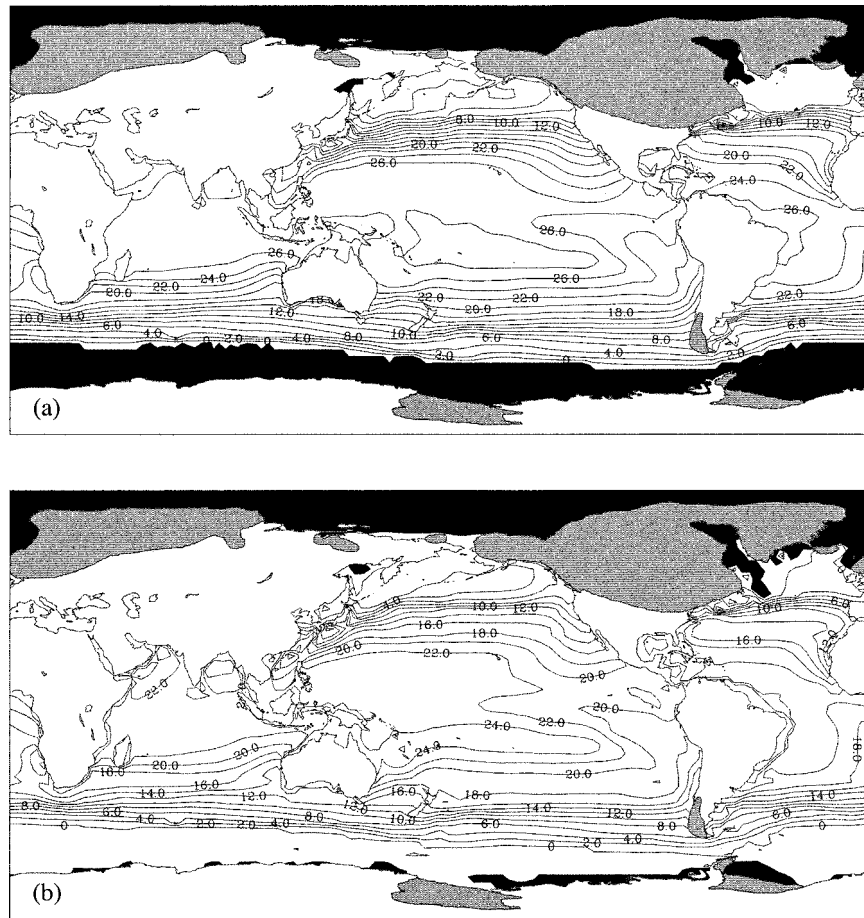


FIG. 2. Mean DJF SST for the (a) CLIMAP and (b) modified CLIMAP simulations. Contour interval is 2°C . Black shading denotes the seasonal mean sea ice (-1.8°C) extent. Gray shading denotes the approximate extent of the LGM ice sheets.

b. Sea surface temperatures

The monthly mean SSTs for the CLIMAP simulation were derived using the February and August CLIMAP SST reconstructions. The seasonal cycle for the CLIMAP SST data is typically assumed to be sinusoidal at each grid point. Examination of the present-day seasonal cycle in the Shea et al. (1992) SST climatology shows sinusoidal variability at many mid- to high-latitude locations, but significant deviations from a sinusoid in the Tropics where bimodal peaks or skewed sinusoids are common. Thus, in the current study the monthly mean CLIMAP SST data were computed by extrapolating the CLIMAP February and August data at each grid point using the month-to-month fractional change in the present-day SST. This method preserves the present-day seasonal cycle at each grid point, which is reasonable since present-day and LGM solar forcing are very similar (see Table 1). Imposing the present-day seasonal cycle results in only minor differences ($<0.5^{\circ}\text{C}$) in the SST annual and seasonal means in the deep Tropics (20°S – 20°N). The mean December–February (DJF) and June–August (JJA) CLIMAP SST are shown in Figs. 2a and

3a, respectively. Tropical SSTs are mostly 26°C or greater with the summer SST maxima exceeding 28°C in the tropical Pacific Ocean. Sea ice ($\text{SST} = -1.8^{\circ}\text{C}$) extent in the CLIMAP reconstruction shows very little seasonal variability in the Southern Hemisphere. Seasonal changes in the Northern Hemisphere sea ice are also slight with greater seasonality in the sub-Arctic region of the North Atlantic.

For the modified CLIMAP simulation, we found that modifying the CLIMAP SSTs uniformly throughout the seasonal cycle a sufficient means to both cool the tropical SSTs and reduce the high-latitude sea ice extent relative to CLIMAP. In previous studies, Rind (1986) cooled the CLIMAP SSTs by 2°C globally. Yin and Battisti (2001) applied a 3°C cooling to the modern SSTs in the deep Tropics. In the current study, the SST boundary conditions for the modified CLIMAP simulation were derived by first cooling the annual mean CLIMAP SSTs by 4°C in the tropical equatorial belt (30°N – 30°S) based on a broad consensus from available proxy information. This magnitude of SST cooling is greater than that suggested by many ocean-based proxy meth-

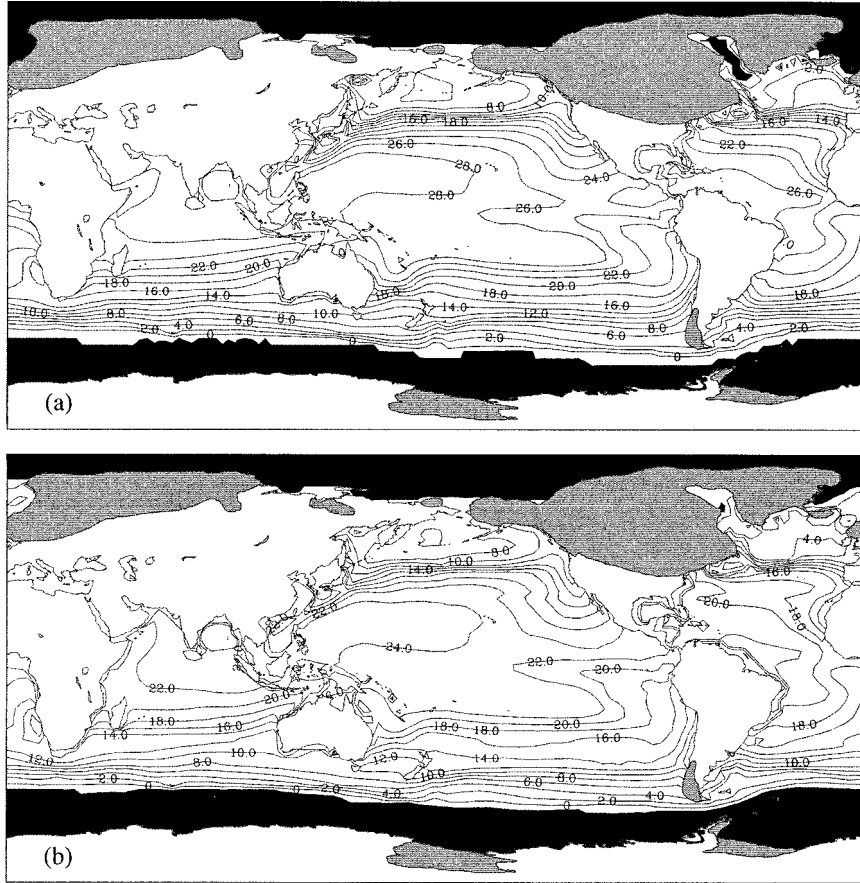


FIG. 3. The same as in Fig. 2 except for JJA.

ods and comparable to or slightly less than estimates from land-based paleothermometry. From 30° – 40° latitude, the SSTs were linearly interpolated to the annual mean CLIMAP SST values, with CLIMAP values retained from 40° – 90° latitude. Next, the present-day annual mean SST field was subtracted from the cooled annual mean CLIMAP SSTs and the difference field applied to each of the present-day monthly mean SSTs to obtain the modified CLIMAP monthly mean SSTs. Thus, the magnitude of cooling in the modified CLIMAP SSTs is related to the magnitude of cooling of the annual mean CLIMAP SSTs relative to present day. This methodology damps the amplitude of the CLIMAP seasonal cycle such that DJF (JJA) SSTs are warmer (cooler) than CLIMAP.

The mean DJF and JJA SSTs for the modified CLIMAP simulation are shown in Figs. 2b and 3b, respectively. In addition to the tropical cooling, note the amplified sea ice seasonal cycle in the Southern Hemisphere. During austral summer (DJF), sea ice retreats to near the Antarctic coast, similar to LGM reconstructions based on diatom analysis (Crosta et al. 1998b). In the Northern Hemisphere, mean winter sea ice extent is similar for the two LGM runs. However, SSTs are somewhat warmer in the North Atlantic and North Pacific in

the modified CLIMAP distribution and there is much less sea ice during mid-to-late winter (January/February) when sea ice typically reaches maximum extent (not shown).

Each model simulation was integrated for 18 yr with monthly mean output. The first 3 yr of each simulation were discarded as spinup and long-term annual and seasonal (JJA and DJF) averages were computed from the remaining output. In order to examine high-frequency modes of atmospheric variability (e.g., transient eddy kinetic energy), the final 5 yr of each 18-yr model run were identically repeated to obtain twice-daily output from CCM3.

3. Results

a. Global and annual means

The global and annual means of several model output fields from the present-day simulation, the CLIMAP simulation (CL hereafter), and the modified CLIMAP run (modCL hereafter) are listed in Table 2. The global and annual mean parameters from the two LGM simulations were compared using the Student's *t* test and found to be different at the 99.9% significance level.

TABLE 2. Global and annual mean properties from the 15-yr present-day, CLIMAP, and modified CLIMAP simulations.

	Present day	CLIMAP	Modified CLIMAP
2-m temperature (K)	286.1	281.6	279.0
Cloud fraction (%)			
Total	59.29	58.32	58.08
Low	34.98	34.2	32.63
Middle	21.07	21.46	25.0
High	34.81	32.94	31.48
Ground albedo	0.15	0.21	0.19
Planetary albedo	0.33	0.35	0.34
Net surface solar radiation ($W m^{-2}$)			
All sky	170.72	168.15	173.75
Clear sky	220.78	212.65	217.92
Outgoing longwave radiation ($W m^{-2}$)			
All sky	236.2	235.5	228.8
Clear sky	265.7	262.0	255.9
Longwave cloud forcing ($W m^{-2}$)	29.5	26.5	27.1
Latent heat flux ($W m^{-2}$)	90.0	84.78	74.19
Sensible heat flux ($W m^{-2}$)	20.16	22.97	24.24
Precipitation ($mm day^{-1}$)	3.09	2.91	2.55

With prescribed modern SSTs, the global mean 2-m air temperature in the present-day simulation is 286.1 K, which is approximately $1.1^{\circ}C$ cooler than that obtained from the 300-yr fully coupled Climate System Model (CSM, version 1) present-day simulation described by Boville and Gent (1998). For the LGM, the global mean 2-m temperature is 281.6 K in the CL run and 279.0 K in the modCL run. The difference in mean 2-m temperature over the oceans alone for the modCL and CL runs is $1.93^{\circ}C$, which accounts for 75% of the difference in global mean 2-m temperature between the two runs. This is comparable to the fractional coverage of ocean area and shows that the cooling in the modCL global mean 2-m temperature relative to the CL run is largely due to the imposed SSTs.

Atmospheric cooling at the LGM generally coincides with reduced mean cloud fractions. The exception is at midlevels where the mean cloud fraction is largest (25%) in the modCL simulation due to a change in the depth of atmospheric convection. As Rind (1998) notes, cooler tropical SSTs result in convection that peaks at midtropospheric levels, increasing the midlevel cloud amount. The clear sky net surface solar radiation values are indicative of the differences in surface albedo for the three model runs. With the continental ice sheets and extensive sea ice cover contributing to a high surface albedo, the CL clear sky net surface solar radiation is least among the model runs. The reduced sea ice extent in the modCL simulation contributes to a slightly lower surface albedo and approximately $5 W m^{-2}$ increase in clear sky net surface solar radiation relative to CL. In general, the cooler LGM climate, influenced by the continental ice sheets, lower trace gas concentrations, and cooler SSTs, reduces the top-of-the-atmosphere longwave radiation flux, both with and with-

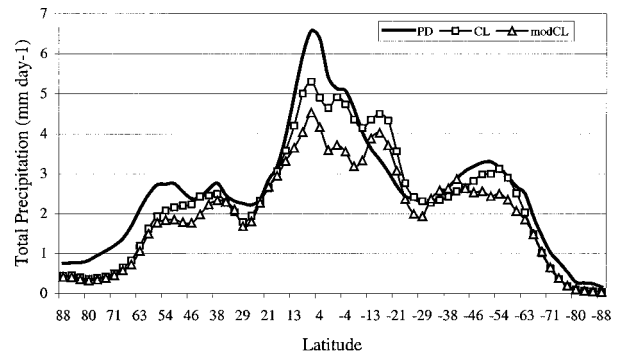


FIG. 4. Zonally averaged 15-yr annual mean precipitation rate ($mm day^{-1}$) for the present-day (solid, bold), CL (square), and modCL (triangle) simulations.

out clouds, relative to present day. The net effect of cooled tropical SSTs in the modCL run is a reduction of $8-10 W m^{-2}$ in the outgoing longwave radiation relative to present. The longwave cloud forcing in the modCL run is slightly greater than in CL, most likely due to the contribution from increased midlevel cloud.

The zonal-mean distributions of annual precipitation for the present-day, CL, and modCL simulations are shown in Fig. 4. LGM precipitation is reduced relative to present at all latitudes except the Southern Hemisphere low latitudes (approximately $10^{\circ}-25^{\circ}S$), due in part to increased precipitation along the South Pacific convergence zone (SPCZ) during the LGM as others have noted (e.g., Yin and Battisti 2001). The changes in the SPCZ are explored further toward the end of this section. The annual mean precipitation in the modCL simulation is reduced relative to CLIMAP throughout much of the low- and midlatitudes with very little change at latitudes poleward of $60^{\circ}-65^{\circ}$. Averaged globally, the modCL annual precipitation rate is $2.55 mm day^{-1}$, which is a 12% and 19% reduction in global mean precipitation relative to CL and present day, respectively (Table 2). The latent heat fluxes in the modCL run are decreased by similar percentages.

b. Large-scale atmospheric response to SST forcing

Many previous modeling studies have compared the LGM (CLIMAP) and present-day climates. The remainder of the current study focuses primarily on the two LGM runs to isolate the sensitivity of the LGM atmosphere to changes in the CLIMAP SST and sea ice boundary conditions, which are shown as zonal means for DJF and JJA in Fig. 5. Cooling (warming) the low (high) latitude SSTs in the modCL run effectively reduces the meridional temperature gradient. Although the large-scale atmospheric response to the SST and sea ice forcing is most pronounced during DJF, especially in the Northern Hemisphere as others have noted, it will be shown that significant large-scale circulation changes are also evident in the Southern Hemisphere.

The 15-yr-mean DJF modCL 2-m air temperatures

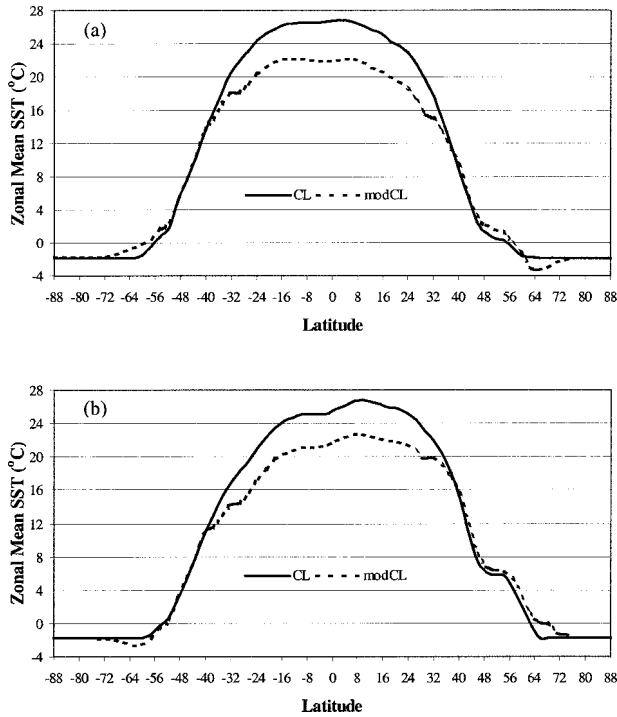


FIG. 5. The 15-yr-mean (a) DJF and (b) JJA zonal-mean SST ($^{\circ}\text{C}$), including sea-ice-covered grid points, for the CL (solid) and modCL (dashed) simulations.

are shown in Fig. 6a with the differences relative to the CL run in Fig. 6b. The corresponding fields for JJA are shown in Figs. 7a,b. The shaded regions in these and subsequent difference plots indicate statistical significance at the 99.9% level using the Student's t test. Prominent in the winter 2-m temperature difference fields are the large positive 2-m temperature anomalies over portions of the extratropical ocean basins. In the Northern Hemisphere during DJF, the anomalies exceed 12°C over the North Atlantic and 20°C over the Sea of Okhotsk in eastern Russia (Fig. 6b). During austral winter (JJA), the 2-m temperature anomalies exceed 8°C over portions of the South Pacific (Fig. 7b). These are due primarily to the prescribed SSTs. For example, in the Sea of Okhotsk and the western North Pacific, the modCL SSTs are $1^{\circ}\text{--}4^{\circ}\text{C}$ warmer through the boreal winter months resulting in less extensive sea ice in this region than in the CL run, particularly in late winter. Warmer SSTs and the reduced sea ice in the modCL simulation allow greater fluxes of sensible heat ($>100\text{ W m}^{-2}$) and latent heat ($>50\text{ W m}^{-2}$) to the lower troposphere relative to CL. This phenomenon also occurs in the high-latitude ocean basins during the summer months, although the 2-m temperature anomalies are much smaller in magnitude than in winter, even in the Southern Ocean despite the substantial difference in summer sea ice extent between the two LGM simulations.

The relatively warm 2-m temperatures over portions of the high-latitude oceans in the modCL run have a

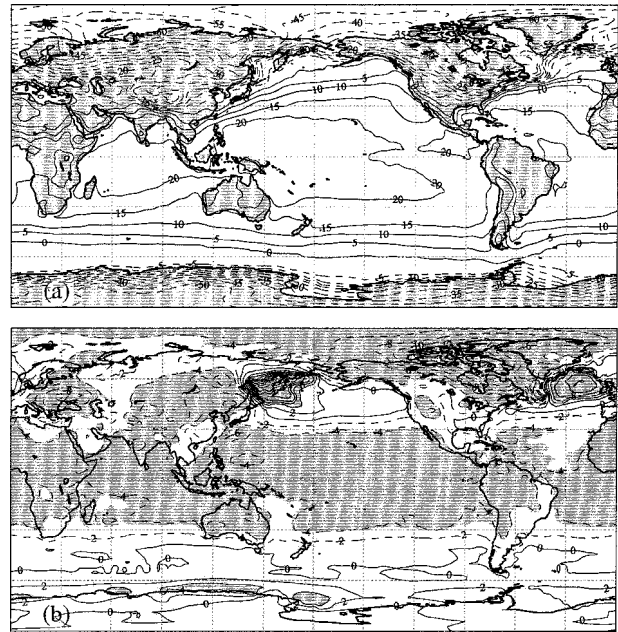


FIG. 6. The 15-yr-mean DJF 2-m temperature for the (a) modCL simulation and (b) modCL minus CL difference. Contour interval is 5°C in (a) and 2°C in (b). Negative contours are dashed in (b), and shaded regions indicate statistical significance at the 99.9% level using the Student's t test.

significant impact on the wintertime Northern Hemisphere atmospheric mass field. Figure 8a shows the DJF mean sea level pressure (MSLP) for the modCL run with the surface pressure difference (modCL minus CL) in Fig. 8b. In the modCL run, the Aleutian low in the North Pacific is located slightly westward of its position in the CL run. The surface pressure anomalies show

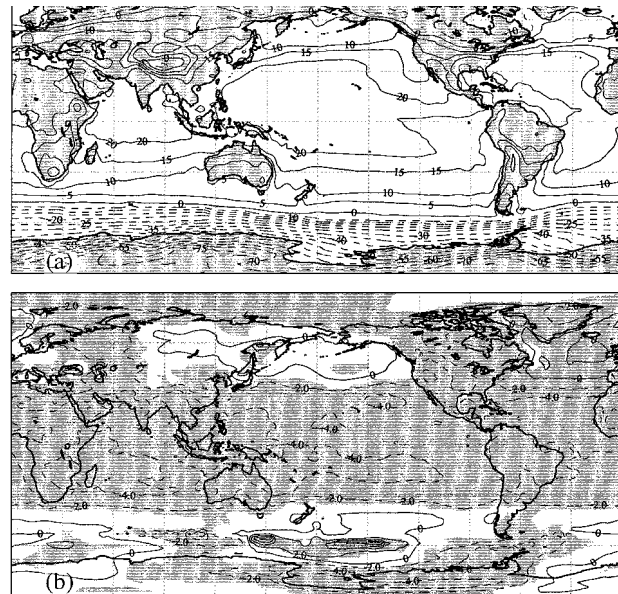


FIG. 7. The same as in Fig. 6 except for JJA.

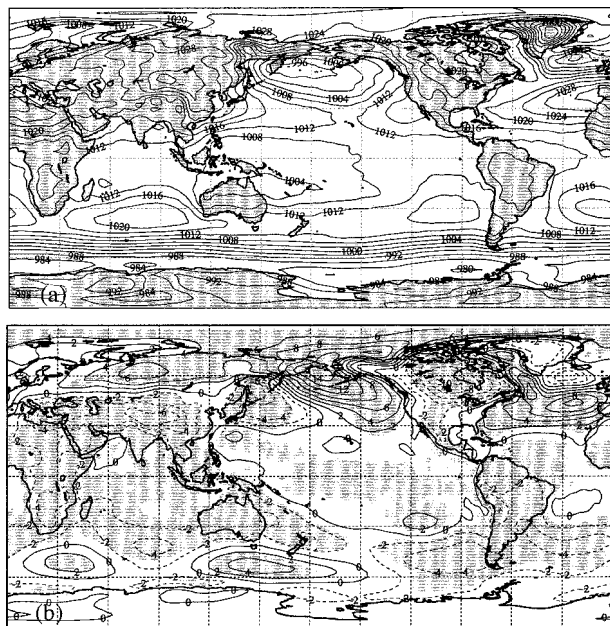


FIG. 8. The 15-yr-mean DJF sea level pressure for the (a) modCL simulation and (b) modCL minus CL surface pressure difference. Contour interval is 4 hPa in (a) and 2 hPa in (b). Negative contours are dashed in (b), and shaded regions indicate statistical significance at the 99.9% level using the Student's t test.

large (>8 hPa) statistically significant pressure decreases over the Sea of Okhotsk with a broad area of pressure increases in the central and eastern North Pacific. The anomaly pattern results from thermal gradients having opposing effects. The decreased meridional SST gradient in the modCL simulation results in a general weakening of the wintertime Aleutian low except in the western North Pacific where the juxtaposition of relatively warm temperatures over the Sea of Okhotsk and cold continental temperatures substantially increases the local baroclinicity (see Fig. 6).

Similarly, over the modCL North Atlantic large (>200 W m^{-2}) sensible and latent heat flux anomalies contribute to a stronger Icelandic low in the modCL run (Fig. 8b). The surface pressure anomaly pattern in the North Atlantic resembles the positive phase signature of the contemporary North Atlantic Oscillation, with negative anomalies in the vicinity of the Icelandic low and positive anomalies in the central Atlantic. The latter are due to a westward shift, rather than a change in magnitude, of the subtropical Azores high pressure in the modCL run. The surface pressure anomaly couplet may augment the warm 2-m temperatures in portions of the North Atlantic since the deeper Icelandic low and stronger Azores high increase the meridional pressure gradient, which enhances the westerly or southwesterly low-level wind flow and warm advection. Figure 9 shows that the near-surface westerly winds in the modCL run have increased by $5\text{--}7$ m s^{-1} over the North Atlantic southeast of Greenland.

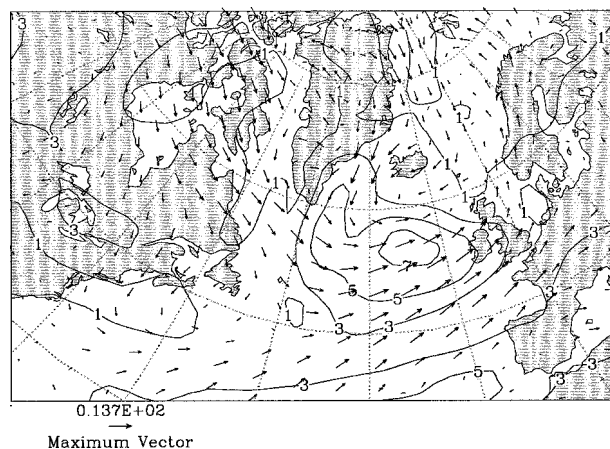
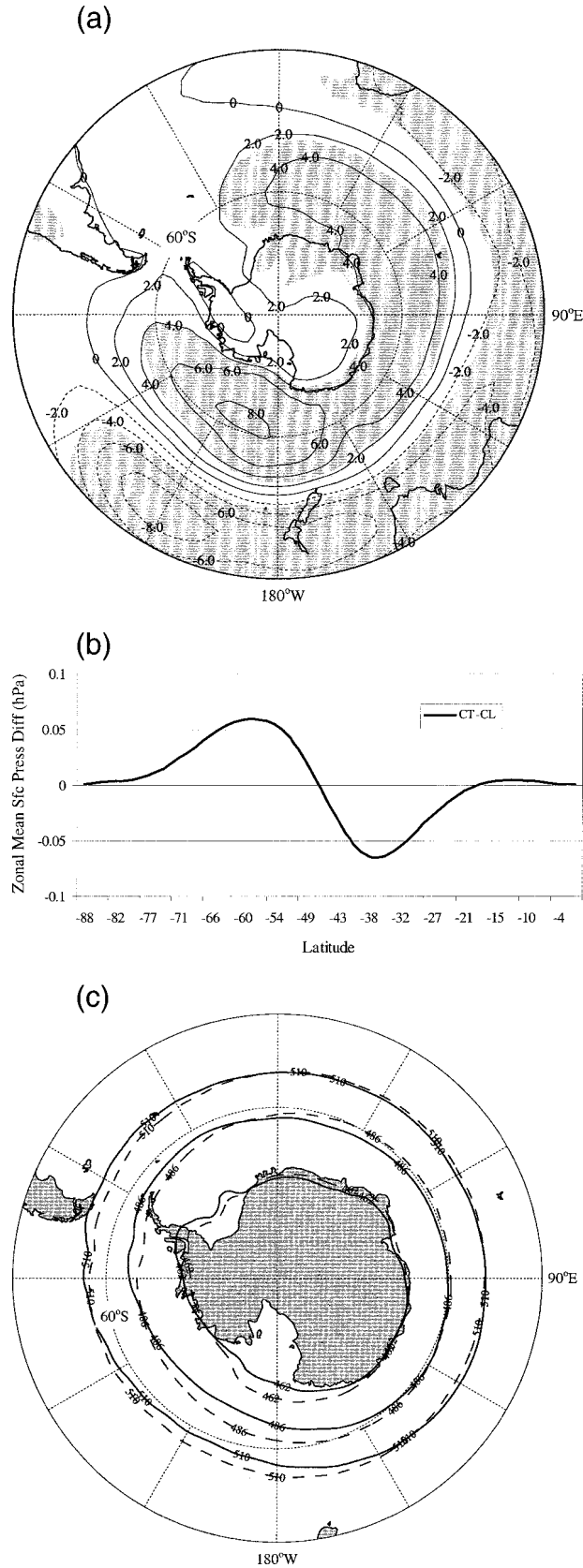


FIG. 9. The 15-yr-mean DJF near-surface (lowest model sigma level) wind vectors for the modCL simulation. Vector magnitudes and the contoured scalar difference (modCL minus CL) are in m s^{-1} .

In the Southern Hemisphere during austral summer, the surface pressure anomalies along the westerly wind belt resemble a wavenumber-2 pattern, with alternating regions of positive and negative pressure differences (Fig. 8b). While the mean summer position of the circumpolar trough (using the 1000-hPa contour) is very similar for the two LGM runs, the anomalies are the result of weaker ($2\text{--}4$ hPa) subtropical high pressure centers and a relaxed meridional pressure gradient in the modCL simulation. During austral winter, the most pronounced large-scale mass field differences occur in the Southern Hemisphere, particularly over the southern oceans as shown in Fig. 10a. The zonal-mean surface pressure anomalies (Fig. 10b), weighted with respect to latitude, indicate that the circumpolar pressure anomaly pattern represents a meridional mass exchange between subtropical high pressure and the circumpolar trough, which results from the reduced meridional temperature gradient in the modCL simulation. It is not apparent whether the extreme surface pressure anomaly couplet in the South Pacific is preferentially located.

At upper levels over the Southern Hemisphere mid and high latitudes, the 500-hPa geopotential height field in the modCL simulation responds dynamically to surface thermal forcing. Over the South Pacific sector of circumpolar ocean (60°S , 180°), and to a lesser degree the South Indian sector (60°S , 30°E), 500-hPa heights have increased in the modCL simulation (Fig. 10c) in the vicinity of positive near-surface temperature anomalies (see Fig. 7b). Warming of the atmospheric column causes the 1000–500-mb layer thickness to increase by $5\text{--}10$ dam in the South Indian Ocean sector and $20\text{--}40$ dam in the South Pacific sector (not shown). The 500-hPa heights and 1000–500-mb layer thickness decreases relative to CL downstream near the Antarctic Peninsula and Drake Passage where the near-surface temperatures are colder in the modCL run.

Generally, the midlatitude atmospheric circulation is



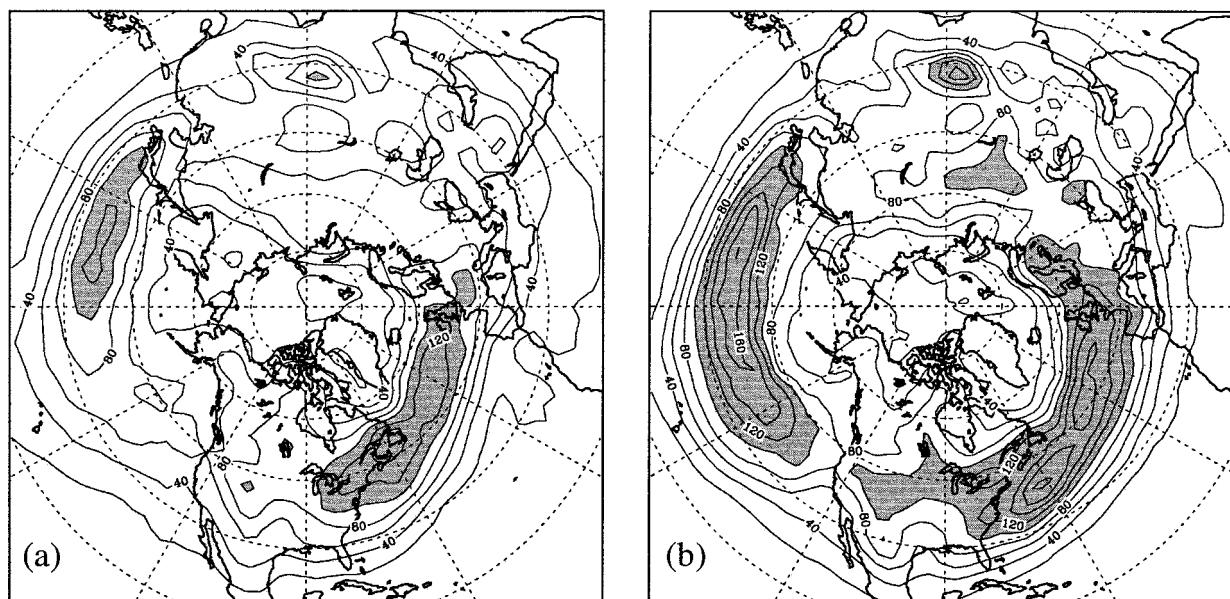


FIG. 12. The 15-yr-mean DJF transient eddy kinetic energy for the (a) modCL simulation and (b) CL simulation. Contour interval is $20 \text{ m}^2 \text{ s}^{-2}$ with values greater than $100 \text{ m}^2 \text{ s}^{-2}$ shaded.

the Okhotsk Sea and extending downstream to North America. The sea ice configurations in the CL and modCL LGM simulations are analogous to the “heavy” and “light” sea ice experiments by Honda et al. (1999). The surface pressure and 500-hPa height anomalies from the Sea of Okhotsk to the Bering Strait indicate that the local and near-field dynamic response is consistent with their findings, although the presence of the Laurentide Ice Sheet undoubtedly affects the downstream response over North America.

The deamplification of the 500-hPa long-wave pattern suggests a weaker Northern Hemisphere storm track, which is more clearly seen in a comparison of the mean DJF 500-hPa transient eddy kinetic energy (TEKE) for the two LGM runs (Fig. 12). The TEKE was computed by applying the Blackmon medium-band filter (Blackmon 1976) to 5 yr of twice-daily CCM3 output to capture the 2.5–6-day variance in the 500-hPa kinetic energy derived from the zonal and meridional winds. In the modCL run, the Northern Hemisphere trans-Pacific storm track is weakened and zonally truncated, with transient eddy activity largely confined to the western and central Pacific basin (Fig. 12a). Thus, eddy fluxes of heat and moisture are reduced from the eastern Pacific to North America, which contributes to the dramatic 2-m temperature cooling over the Laurentide Ice Sheet and Greenland in the modCL run (see Fig. 6). The North Atlantic 500-hPa storm track is also truncated and weaker relative to CL (Fig. 12b) with the axis of maximum TEKE shifted northward, extending from the eastern Great Lakes and Newfoundland to western Europe. Similarly, during the Southern Hemisphere winter, the circum-Antarctic 500-hPa TEKE is also substantially re-

duced in the modCL simulation (not shown), consistent with the decreased meridional 500-hPa height gradient.

The weaker Northern Hemisphere storm tracks in the modCL simulation directly affect the winter precipitation accumulation over the continental ice sheets. Figures 13a and 13b show the modCL 15-yr-mean DJF monthly mean precipitation and the difference relative to CL, respectively. Precipitation is significantly reduced over the central and eastern Pacific and over much of North America in the modCL simulation. Likewise, reduced 500-hPa TEKE and the northward shift of the North Atlantic storm track result in significant basin-wide precipitation decreases except in the vicinity of the intensified Icelandic low.

In the Southern Hemisphere, precipitation is decreased significantly over the circumpolar oceans during summer and winter (not shown), consistent with the reduction in transient eddy activity. At low latitudes in the modCL simulation, significant precipitation decreases occur during DJF over much of the Tropics with the exception of Amazonia and the tropical North Atlantic, the SPCZ region east of Australia, the Hawaiian Islands, southeastern Africa, and the western Indian Ocean basin. The distribution of low-latitude precipitation anomalies in Fig. 13b generally agrees with regions identified by Ropelewski and Halpert (1989) with statistically significant precipitation–cold phase El Niño–Southern Oscillation relationships.

c. Summer monsoon response

In addition to the changes to the large-scale atmospheric circulation in response to the SST forcing, pro-

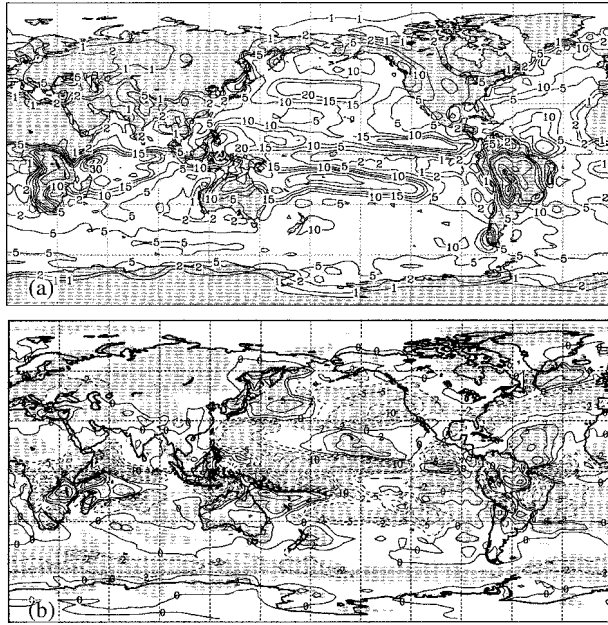


FIG. 13. The 15-yr-mean DJF monthly mean precipitation for the (a) modCL simulation and (b) modCL minus CL difference. Contours are 1, 2, 5, 10, 15, 20, 30, 40, 50, and 60 cm month^{-1} in (a) and $\pm 0, 2, 5, 10, 15, 20,$ and 30 cm month^{-1} in (b). Negative contours are dashed in (b), and shaded regions indicate statistical significance at the 99.9% level using the Student's t test.

nounced regional-scale changes occur in the Northern Hemisphere monsoon circulations because of the increased land–ocean temperature difference in the modCL simulation. Figure 14a shows the modCL minus CL differences in the surface pressure and near-surface wind fields over the Asian monsoon region during JJA. Negative surface pressure anomalies occur over the landmasses, with the largest decrease (6 hPa) over central Saudi Arabia and the Tibetan Plateau. The surface pressure has increased slightly in the central and western Indian Ocean in the vicinity of the Mascarene high. Consequently, the cross-equatorial near-surface flow is increased over the western Indian Ocean with the Somali jet nearly 50% (7 m s^{-1}) stronger in the modCL run, representing the largest magnitude increase of the near-surface wind during JJA. The enhanced low-level flow is accompanied by increased monsoon precipitation over much of the region (Fig. 14b). The increased land–ocean temperature difference in the modCL run also leads to a similar response, though smaller in magnitude, in the monsoon flow over the southwestern United States (not shown).

The increased monsoon flow and precipitation in the modCL has a direct impact on the mean meridional circulation as illustrated by the JJA zonal-mean streamfunction in Fig. 15. Driven largely by Asian monsoon convection and latent heat release, the JJA Southern Hemisphere Hadley cell is approximately 20% more intense than in CL, with no appreciable change in size or position. Rind (1998) notes that Hadley cell intensity

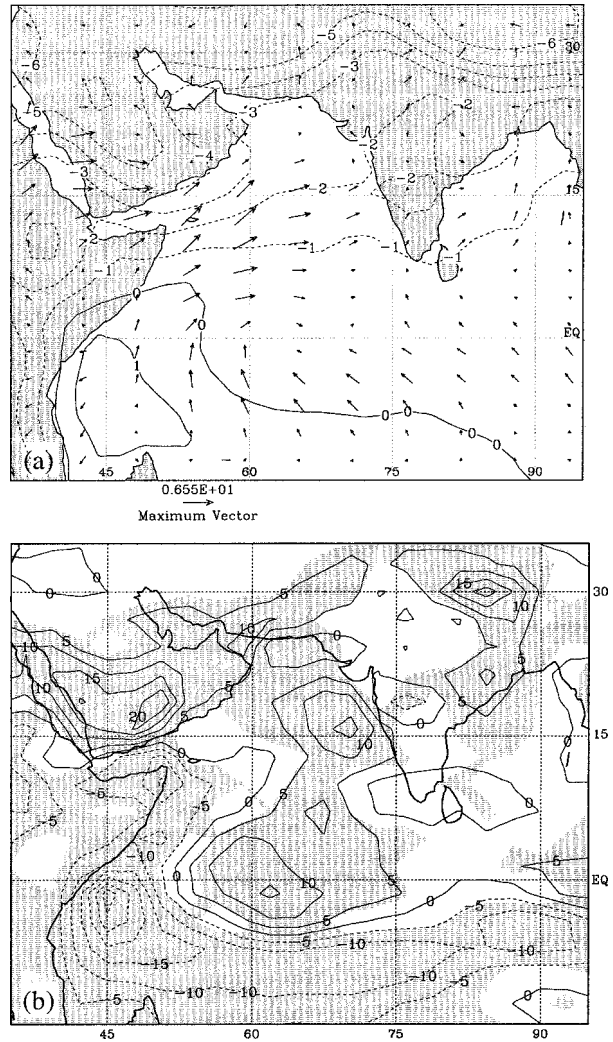


FIG. 14. The 15-yr-mean JJA modCL minus CL surface pressure difference and near-surface (lowest model sigma level) (a) vector wind difference and (b) modCL minus CL precipitation difference. Contours are $\pm 2 \text{ hPa}$ and vector magnitudes are in m s^{-1} in (a). Contours are $\pm 5 \text{ cm month}^{-1}$ in (b).

is governed by the latitudinal temperature gradient. The current results for JJA corroborate Rind's findings in as much as the latitudinal temperature gradient is augmented by the land–ocean temperature contrast. Elsewhere, the Northern Hemisphere Hadley cell and the midlatitude Ferrell cells in both hemispheres are weaker in the modCL run indicating that the effect of the increased land–ocean temperature contrast is most pronounced in the Asian monsoon region.

d. South Pacific convergence zone

The annual and zonal precipitation distributions shown previously in Fig. 4 suggest that the SPCZ was an exceptional feature in the cooler and drier LGM climate. Vincent (1994) gives a thorough review of the

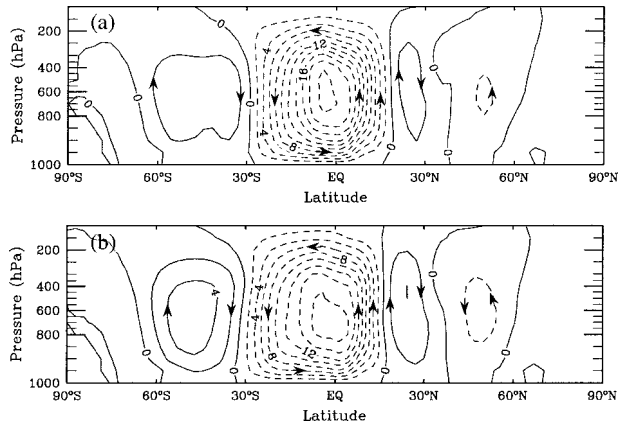


FIG. 15. The 15-yr-mean JJA zonal-mean streamfunction for the (a) modCL simulation and (b) CL simulation. Contour interval is $2 \times 10^{10} \text{ kg s}^{-1}$ with negative contours dashed.

contemporary SPCZ, which consists of an axis of persistent low-level moisture convergence with associated convection extending from New Guinea east-southeastward to the central South Pacific along a trough of low pressure. The SPCZ is most pronounced during austral summer. Figure 16 shows the 15-yr-mean DJF MSLP for the present-day, CL, and modCL simulations. Also shown is the axis of maximum low-level wind

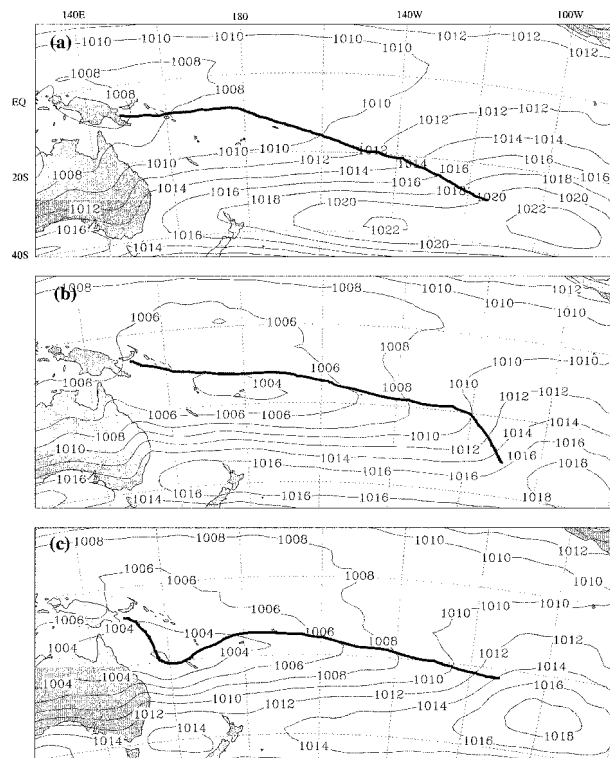


FIG. 16. (a) Present-day, (b) CLIMAP, and (c) modified CLIMAP 15-yr-mean DJF mean sea level pressure (hPa). Heavy solid line denotes the axis of maximum low-level (surface to 700 hPa) convergence along the SPCZ.

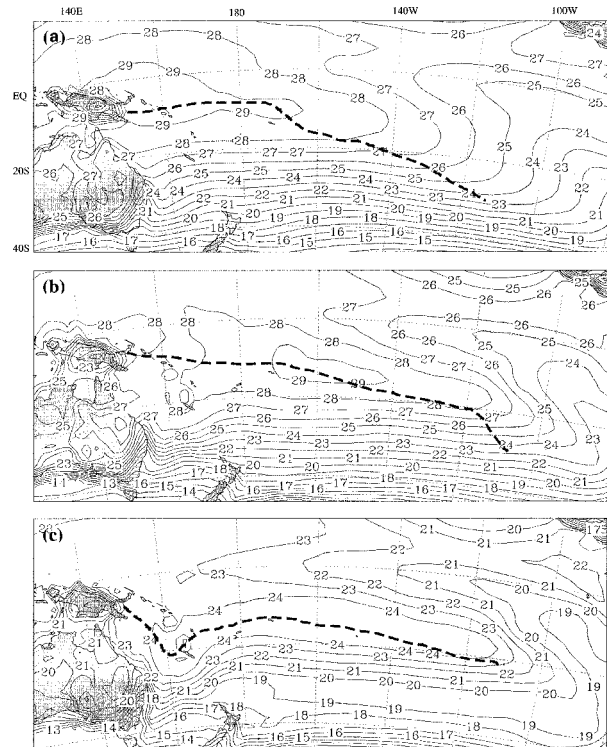


FIG. 17. (a) Present-day, (b) CLIMAP, and (c) modified CLIMAP 15-yr-mean DJF surface temperature ($^{\circ}\text{C}$). Heavy dashed line denotes the axis of maximum precipitation along the South Pacific convergence zone.

convergence (averaged from the surface to 700 hPa) along the SPCZ in each simulation. The structure and intensity of the DJF SPCZ differ somewhat for the three simulations. The present-day simulation captures the characteristic zonal (tropical) and diagonal (subtropical) segments of the SPCZ extending from low pressure over New Guinea (Fig. 16a). In the CL simulation, low pressure is centered farther east near Fiji (15°S , 175°E) and the axis of maximum low-level wind convergence has a more zonal orientation than in the present-day run except for the distinct diagonal segment in the eastern South Pacific (Fig. 16b). The modCL SPCZ (Fig. 16c) consists of relatively strong low pressure (1002 hPa) positioned near Australia (19°S , 158°E) with a nearly zonal trough and convergence axis across the central South Pacific.

The zonal portion of the contemporary DJF SPCZ is thought to be maintained by low-level thermal forcing due to SST gradients and land–ocean temperature contrasts, while the SST distribution and interactions with midlatitude synoptic disturbances most likely influence the orientation and intensity of the diagonal segment (Vincent 1994). Low-level thermal forcing appears to significantly influence the SPCZ in the current simulations. Figure 17 shows the surface temperature distributions for the present-day and LGM simulations. Superimposed is the SPCZ axis of maximum precipitation

for each model run, which is roughly coincident with the axis of maximum low-level wind convergence in Fig. 16. In each simulation, the SPCZ orientation follows closely the axis of maximum surface temperature. The temperature distributions in Fig. 17 also indicate that the warmest SSTs in the LGM simulations are located farther eastward to the central equatorial South Pacific. Thus, while the magnitudes of meridional and longitudinal temperature gradients across the equatorial South Pacific are similar in the present-day and LGM simulations, the distributions of the temperature gradients differ. Increased precipitation along the SPCZ at the LGM is consistent with the three- to fourfold increase in low-level convergence relative to present day (not shown). While the precise relationship between the SPCZ intensity and the distribution of SST gradients is unclear, it is apparent that the distribution of the surface temperature gradients has a first-order influence on the SPCZ with little influence from midlatitude synoptic systems. This is particularly evident for the modCL simulation where midlatitude transient eddy activity is substantially reduced in accord with the reduced meridional temperature gradient.

4. Discussion

Previous GCM experiments have been configured to test the effects of increased (decreased) latitudinal temperature gradients in cold (warm) climate scenarios (e.g., Rind 1998). In the present study, modifications to the LGM ocean boundary conditions both at low and high latitudes based on the consensus from a significant body of land- and ocean-based proxy data tests the climate sensitivity within part of the boundary forcing parameter space. That is, cooling the CLIMAP tropical SSTs by 4°C and reducing CLIMAP winter (summer) sea ice in the Northern (Southern) Hemisphere have two principal but opposite effects on the lower boundary forcing at the LGM: 1) reduced meridional temperature gradient, and 2) increased land–ocean temperature difference. The former induces a large-scale atmospheric response, while the response to the latter forcing mechanism is primarily regional.

The reduced meridional temperature gradient in the modCL simulation directly affects the extratropical atmospheric circulation in both hemispheres and is most pronounced in the winter hemisphere. For instance, the meridional midtropospheric geopotential height gradient is significantly reduced and the jet-level zonal flow is diminished, in accord with the thermal wind relationship. Rind (1986) notes that increased meridional temperature gradients in paleoclimate simulations lead to increased baroclinic energy generation. Consistent with this but in the opposite sense, the decreased meridional temperature gradients in the modCL simulation lead to substantially decreased transient eddy kinetic energy at midlatitudes, which in turn contributes to the significant decreases in winter midlatitude precipitation.

Previous global modeling studies that attempt to reconcile the LGM climate with proxy observations focus on modified tropical SSTs with little or no consideration of the effects of explicitly modified sea ice. The results from the current study show that in both seasons reduced sea ice has a substantial impact primarily on the regional atmospheric circulation. The modified CLIMAP SSTs increase the land–ocean temperature difference, which (in opposition to the reduced meridional temperature gradient) leads to a locally intensified atmospheric circulation. For instance, compared with the CLIMAP simulation the winter Icelandic low is significantly stronger in response to warmer SSTs and reduced sea ice in the North Atlantic. Rind (1998) finds that the Icelandic low is not particularly sensitive to changes in the latitudinal (i.e., large-scale) temperature gradient, but the current study shows a pronounced response to *locally* increased baroclinicity via enhanced sensible and latent heat fluxes from a warm ocean surface adjacent to a cold landmass. Similarly in the North Pacific, the weakened winter Aleutian low in our experiment is in agreement with previous studies (Rind 1998; Yin and Battisti 2001), although the reduced sea ice acts to partially offset the effect of the reduced meridional temperature gradient. To better isolate the effects of modified sea ice from those resulting from changing the SSTs both at low and high latitudes, we conducted an additional LGM sensitivity simulation using cooled tropical SSTs (as in the modCL run), but retained the CLIMAP sea ice distribution at high latitudes. The large-scale atmospheric circulation resulting from the SST forcing in this sensitivity run (not shown) was very similar to the large-scale atmospheric response to the modCL SSTs, but lacking the local intensification of the Aleutian and Icelandic lows evident in the modCL run. This substantiates what we infer from the modCL simulation, that reduced high-latitude sea ice at the LGM has an important influence on the regional atmospheric circulation, while the cooler tropical SSTs primarily affect the large-scale circulation. With regard to LGM climate simulations, these findings underscore the importance of improved sea ice estimates as part of the global reconstruction of LGM SSTs.

Since the ocean boundary conditions in our experiment have been modified based on proxy data, one would expect an improvement over CLIMAP in the comparison between model results and LGM proxy evidence. With regard to the hydrologic cycle, lake-level estimates, pollen and plant macrofossil assemblages, and fossil dunes indicate increased aridity in much of the equatorial Tropics at the LGM, whereas the southwest United States and the Mediterranean region were likely wetter than today (Sarnthein 1978; Street and Grove 1979; Farrera et al. 1999). In the global mean, the modCL simulation in the current study produces less precipitation than the CL run, with most of the reduction occurring in the Tropics as the proxy data indicate. The spatial patterns of precipitation anomalies relative to the

TABLE 3. Annual mean 2-m temperature difference (LGM minus present; °C) from proxy data estimates and CCM3 model output. Differences are negative with one exception (in bold font). Standard deviations and error bars are as listed in the cited study.

Source	Proxy method	Location	Temperature reduction, proxy	modCL (CL) minus PD
Cuffy et al. (1995)	Borehole	72.6°N, 38.5°W	21	21.1 (18.9)
Dahl-Jensen et al. (1998)	Borehole	72.6°N, 37.6°W	21 ± 1.0	20.9 (18.6)
Salamatin et al. (1998)	Borehole	78.28°S, 106.48°E	15	10.1 (9.5)
Miller et al. (1997)	Emu eggshells	28.5°S, 137°E	9	5.8 (2.1)
Thompson et al. (1995)	Ice core $\delta^{18}\text{O}$	9.12°S, 77.62°W	8–12	6 (1.2)
Stute et al. (1992)	Noble gases	28.75°N, 98.5°W	5.2 ± 0.7	8.4 (6.4)
Stute et al. (1995a)	Noble gases	36.6°N, 108.1°W	5.4 ± 0.7	7.7 (4.7)
Stute et al. (1995b)	Noble gases	7°S, 41.5°W	5.4 ± 0.6	5.8 (1.7)
Weyhenmeyer et al. (2000)	Noble gases	23.5°N, 58°E	6.5 ± 0.6	7.2 (2.7)
Colhoun et al. (1994)	Pollen	42.0°S, 145.5°E	5–6.5	3.6 (3.1)
Colinveaux et al. (1996)	Pollen	0.27°N, 66.7°W	5–6	6 (1.3)
Farrera et al. (1999)*	Pollen	4.91°N, 74.33°W	3–4	6.4 (1.5)
	Pollen	16°S, 69°W	5–7	6.5 (1.6)
	Pollen	6.5°N, 1.41°W	3–4	6.7 (2.2)
	Pollen	3.48°S, 29.57°E	5–6	7 (2.3)
	Pollen	24.43°S, 28.75°E	5–6	6.3 (2.4)
	Pollen	0.03°N, 37.47°E	5.1–8.8	7.5 (2.3)
	Pollen	20.08°S, 43.37°W	5–7	4.8 (1.3)
	Pollen	27.15°S, 109.4°W	2.8	3.4 (0.3)
	Pollen	22.0°N, 100.5°W	1.5–3	6.7 (3.2)
	Pollen	2.17°N, 98.08°E	3	6.9 (2.6)
	Pollen	27.68°N, 85.4°E	6–8	7 (2.9)
	Pollen	5.18°S, 141.63°E	4–5	6.1 (1.5)
Kageyama et al. (2001)*	Noble gases	43.5°N, 1.5°W	5.7	9.2 (6.7)
	Noble gases	48°N, 21°E	8.7	11.4 (7.6)
	Pollen	47°N, 38.5°E	20	9.2 (6.9)
	Pollen	47°N, 6°E	9	10.3 (7.3)
Tarasov et al. (1999)*	Pollen	55°N, 83°E	10 (–3/+5)	10.3 (6.5)
	Pollen	55.17°N, 57.58°E	8 (–2/+9)	13 (10.4)
	Pollen	47.52°N, 111.27°E	10 (–3/+4)	7.8 (4)
	Pollen	51.21°N, 99.45°E	5 (–5/+6)	7.8 (4)
Bard et al. (1997)	Alkenone	3.2°N, 50.4°E	1.5 ± 0.7	5.5 (1.1)
Lyle et al. (1992)	Alkenone	1°N, 139°W	0.5 ± 0.4	5.2 (0.7)
Sikes and Keigwin (1994)	Alkenone	0°, 23°W	1.8 ± 0.6	6.7 (2)
Ternois et al. (2000)	Alkenone	25.02°N, 16.65°W	4.5	9 (4.4)
	Alkenone	21.48°N, 17.95°W	2–2.5	9.8 (5.2)
Guilderson et al. (1994)	Coral Sr/Ca, $\delta^{18}\text{O}$	13.2°N, 59.3°W	5	5.7 (1.3)
Barrows et al. (2000)	Faunal	14.52°S, 117.1°E	0.4	4.2 (0)
	Faunal	33.38°S, 161.61°E	4.2	3.7 (1.2)
	Faunal	44.26°S, 150°E	3.3	3.2 (2.8)
	Faunal	44.78°S, 175.77°W	1.5	2.8 (2.5)
Feldberg and Mix (2002)	Faunal	16.01°S, 76.33°W	6–9	5 (0.7)
Mix et al. (1999)	Faunal	0°, 15°W	5	7.2 (2.5)
	Faunal	10°N, 40°W	2–3	5.3 (1.2)
	Faunal	3°S, 82°W	4–5	5.5 (1.3)
	Faunal	1°S, 110°W	2–3	4.7 (0.6)
Ortiz et al. (1997)	Faunal	42°N, 130.01°W	3.5 ± 1.5	2.2 (2.3)
Lee and Slowey (1999)	Faunal, $\delta^{18}\text{O}$	21.36°N, 158.19°W	2	2.7 (1.4)
Lea et al. (2000)	Mg/Ca	0.3°N, 159.4°E	2.8 ± 0.7	5.8 (1.6)
	Mg/Ca	2.3°N, 91°W	2.6 ± 0.8	4.2 (0.2)
Brathauer and Abelmann (1999)	Radiolaria	43.22°S, 11.74°E	4–5	3.9 (3.6)
	Radiolaria	49°S, 12.7°W	3–4	4.8 (5.5)
Pisias and Mix (1997)	Radiolaria	3.2°N, 101.43°W	3.2	4.4 (0.2)
	Radiolaria	16.45°S, 77.57°W	3.7	4.3 (0.3)

* Proxy temperature estimates are from a compilation of previous studies.

present are very similar for the two LGM runs, which differ mostly in magnitude. It is difficult to determine unambiguously whether the modCL simulation captures better than CL the spatial distribution of precipitation since reconstructions from proxy evidence are often

qualitative and precipitation is highly variable in space and time.

Temperature is a better parameter with which to compare the LGM model runs because quantitative estimates of surface temperature are available from a large number

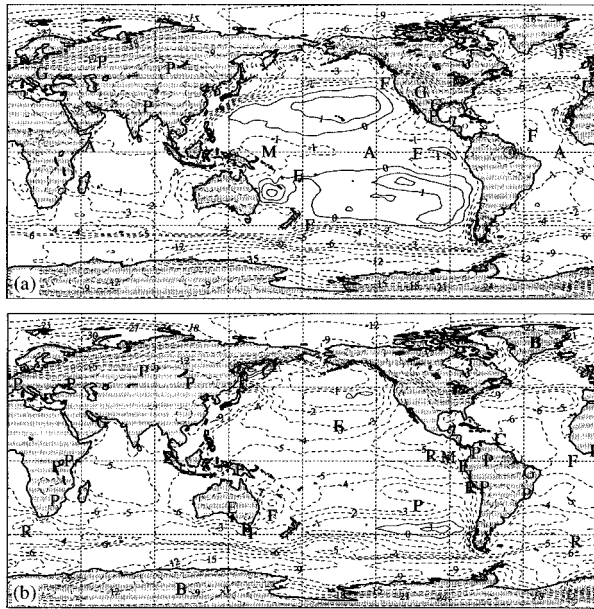


FIG. 18. The 15-yr annual mean 2-m temperature difference: (a) CL minus present day and (b) modCL minus present day. Contours are every 1.0° up to 6°C and every 3°C thereafter; negative contours are dashed. Annotations are plotted at locations of various proxy data types: alkenone (A), borehole (B), coral Sr/Ca ratio (C), emu eggshell (E), faunal/foraminifera (F), noble gases (G), ice core stable isotope (I), Mg/Ca ratio (M), pollen (P), and radiolaria (R).

of proxy sources. Broccoli (2000) compares coupled atmosphere–mixed-layer ocean model output to annual mean surface temperatures estimated from various low-latitude (35°N – 35°S) proxy data. The comparisons show that modeled surface temperatures are close to, but slightly cooler than CLIMAP estimates averaged over the region. In general, the coupled model produces a closer fit to surface temperatures based on ocean proxy methods (e.g., alkenones) than to temperature estimates from terrestrial proxy data. Shinn et al. (2003) perform similar comparisons using output from the NCAR Community Climate System Model (CCSM), with CCM3 as the atmosphere model component. Over land, the area (32°N – 33°S) averaged model prediction of LGM surface temperature cooling is in close agreement with lowland proxy data, though the model does not capture the observed regional variability of cooling. At higher latitudes, the CCSM underestimates the magnitude of annual mean surface temperature cooling at the LGM relative to select proxy locations in Europe, but generally agrees with observed cooling in parts of Siberia.

Following these recent works, we have selected a representative sample of estimates of annual mean surface temperature anomalies from a variety of proxy methods (Table 3). The annual mean 2-m temperature anomalies for CL minus present and modCL minus present are shown Figs. 18a and 18b, respectively, along with the locations of the Table 3 proxy data types that best agree with either the CL or modCL result. The

TABLE 4. Annual mean 2-m temperature anomalies (LGM minus present; $^{\circ}\text{C}$) from proxy data estimates and CCM3 model output. The mean anomalies are negative with the number of data points in each sample in parentheses. Listed in italics are the Student's t test p values comparing the CL and modCL mean temperature anomalies to those estimated from proxy data.

	All points (54)	Land only (31)
Proxy	5.8	7.8
modCL	6.9 (0.18)	8.3 (0.69)
CL	3.5 (0.005)	4.8 (0.014)
	By latitude	
	20°N–20°S (24)	20°–40° (13)
	>40° (17)	
Proxy	4.1	4.8
modCL	5.8 (0.001)	6.4 (0.082)
CL	1.3 (1.0×10^{-6})	2.7 (0.019)
		7.1 (0.31)

model temperature anomalies are computed as the arithmetic mean of values from the five model grid points nearest to a given proxy data location. The mean temperature anomalies for land locations and grouped by latitude belt are given in Table 4. Also listed in Table 4 are the Student's t test p values from statistical comparisons of the model and proxy mean 2-m temperature anomalies. Averaged over all land locations, the modCL temperature anomalies show better agreement than CL with proxy data. However, there is some regional variability. For instance, the modCL temperature anomalies agree closely with the Greenland borehole measurements and a number of the estimates from pollen data. The modCL results are a better fit than CL to the various proxy sources over South America, while the CL results agree more closely with proxy data in western North America and Mexico where the modCL simulation is too cold. Averaged by latitude in the Tropics and subtropics, the modCL results overestimate the LGM cooling, but are closer than CL to the proxy temperature estimates. In mid- and high latitudes (poleward of 40°), the modCL results are in close agreement with proxy estimates, indicating that the cooled tropical SSTs are a primary modulator of the extratropical large-scale atmospheric circulation during the LGM.

Efforts to reconcile modeled and observed LGM temperature and precipitation estimates have been ongoing since the release of the CLIMAP dataset nearly 25 yr ago. Continued scrutiny of proxy techniques (e.g., Crowley 2000) and improvements in model complexity and capability will hopefully lead to consensus and the future release of an updated global LGM SST dataset. Feldberg and Mix (2002) comment that it may be appropriate to apply estimates of LGM SST cooling on a regional rather than global scale. Results from our LGM experiment suggest that, while some regional tuning may be necessary, uniform SST cooling at low latitudes, together with modifications to high-latitude sea ice, appears sufficient to capture to first approximation both regional and large-scale climate changes over much of the globe during the Last Glacial Maximum.

Acknowledgments. This research was funded by National Science Foundation Grant OPP-9905381 to David H. Bromwich. We are grateful to two anonymous reviewers for their critique of this work. Our thanks also to Jim Fastook, David Sugden, and Ross Purves for providing ice sheet data, to Lonnie Thompson and Leonid Polyak for their helpful consultations, and to Rahul George and Raghendra Mupparthy for data processing assistance. Computing support was provided by Grants PAS0045-1 and 36091009 from the Ohio Supercomputing Center and the National Center for Atmospheric Research, respectively.

REFERENCES

- Anderson, J. B., S. S. Shipp, A. L. Lowe, J. S. Wellner, and A. B. Mosola, 2002: The Antarctic Ice Sheet during the Last Glacial Maximum and its subsequent retreat history: A review. *Quat. Sci. Rev.*, **21**, 49–70.
- Armand, L. K., 2000: An ocean of ice—advances in the estimation of past sea ice in the Southern Ocean. *GSA Today*, **10**, 1–7.
- Bard, E., F. Rostek, and C. Sonzogni, 1997: Interhemispheric synchrony of the last deglaciation inferred from alkenone palaeothermometry. *Nature*, **385**, 707–710.
- Barrows, T. T., S. Juggins, P. De Deckker, J. Thiede, and J. I. Martinez, 2000: Sea-surface temperatures of the southwest Pacific Ocean during the Last Glacial Maximum. *Paleoceanography*, **15**, 95–109.
- Beck, J. W., R. L. Edwards, E. Ito, F. W. Taylor, J. Recy, F. Rougerie, P. Joannot, and C. Henin, 1992: Sea-surface temperature from coral skeleton strontium–calcium ratios. *Science*, **257**, 644–647.
- Berger, A., 1978: Long-term variations of daily insolation and Quaternary climatic changes. *J. Atmos. Sci.*, **35**, 2362–2367.
- Blackmon, M. L., 1976: A climatological spectral study of the 500 mb geopotential height of the Northern Hemisphere. *J. Atmos. Sci.*, **33**, 1607–1623.
- Bonan, G. B., 1998: The land surface climatology of the NCAR Land Surface Model coupled to the NCAR Community Climate Model. *J. Climate*, **11**, 1307–1326.
- Boville, B. A., and P. R. Gent, 1998: The NCAR Climate System Model, version one. *J. Climate*, **11**, 1115–1130.
- Bradley, R. S., M. Vuille, D. Hardy, and L. G. Thompson, 2003: Low latitude ice cores record Pacific sea surface temperatures. *Geophys. Res. Lett.*, **30**, 1174, doi:10.1029/2002GL016546.
- Brathauer, U., and A. Abelmann, 1999: Late Quaternary variations in sea surface temperatures and their relationship to orbital forcing recorded in the Southern Ocean (Atlantic sector). *Paleoceanography*, **14**, 135–148.
- Broccoli, A. J., 2000: Tropical cooling at the Last Glacial Maximum: An atmosphere–mixed layer ocean model simulation. *J. Climate*, **13**, 951–976.
- Bush, A. B. G., and S. G. H. Philander, 1999: The climate of the Last Glacial Maximum: Results from a coupled atmosphere–ocean general circulation model. *J. Geophys. Res.*, **104**, 24 509–24 525.
- Cane, M. A., 1983: Oceanographic events during El Niño. *Science*, **222**, 1189–1195.
- Charles, C. D., D. Rind, R. Healy, and R. Webb, 2001: Tropical cooling and the isotopic composition of precipitation in general circulation model simulations of the ice age climate. *Climate Dyn.*, **17**, 489–502.
- CLIMAP Members, 1981: Seasonal reconstruction of the earth's surface at the Last Glacial Maximum. Map and Chart Series, Vol. 36, Geological Society of America, 18 pp.
- Colhoun, E. A., G. van de Greer, and W. K. Mook, 1994: Terrestrial and marine pollen records of the last glaciation from western Tasmania: Do they agree? *Quat. Sci. Rev.*, **13**, 293–300.
- Colinvaux, P. A., P. E. Deoliveira, J. E. Moreno, M. C. Miller, and M. B. Bush, 1996: A long pollen record from lowland Amazonia: Forest and cooling in glacial times. *Science*, **274**, 85–88.
- Crosta, X., J.-J. Pichon, and L. H. Burckle, 1998a: Application of modern analog technique to marine Antarctic diatoms: Reconstruction of maximum sea-ice extent at the Last Glacial Maximum. *Paleoceanography*, **13**, 284–297.
- , —, and —, 1998b: Reappraisal of Antarctic seasonal sea-ice at the Last Glacial Maximum. *Geophys. Res. Lett.*, **25**, 2703–2706.
- Crowley, T. J., 2000: CLIMAP SSTs re-visited. *Climate Dyn.*, **16**, 241–255.
- , and S. K. Baum, 1997: Effect of vegetation on an ice-age climate model simulation. *J. Geophys. Res.*, **102**, 16 463–16 480.
- Cuffey, K. M., G. D. Clow, R. B. Alley, M. Stuiver, E. D. Waddington, and R. W. Saltus, 1995: Large Arctic temperature change at the Wisconsin–Holocene glacial transition. *Science*, **270**, 455–458.
- Dahl-Jensen, D., K. Mosegaard, N. Gundestrup, G. D. Clow, S. J. Johnsen, A. W. Hansen, and N. Balling, 1998: Past temperatures directly from the Greenland Ice Sheet. *Science*, **282**, 268–271.
- de Vernal, A., and C. Hillaire-Marcel, 2000: Sea-ice cover, sea-surface salinity and halo-/thermocline structure of the northwest North Atlantic: Modern versus full glacial conditions. *Quat. Sci. Rev.*, **19**, 65–85.
- Farrera, I., and Coauthors, 1999: Tropical climates at the Last Glacial Maximum: A new synthesis of terrestrial palaeoclimate data. I. Vegetation, lake-levels, and geochemistry. *Climate Dyn.*, **15**, 823–856.
- Fastook, J. L., and J. Chapman, 1989: A map plane finite-element model: Three modeling experiments. *J. Glaciol.*, **35**, 48–52.
- , and M. Prentice, 1994: A finite-element model of Antarctica: Sensitivity test for meteorological mass balance relationship. *J. Glaciol.*, **40**, 167–175.
- Feldberg, M. J., and A. C. Mix, 2002: Sea-surface temperature estimates in the Southeast Pacific based on planktonic foraminiferal species: Modern calibration and Last Glacial Maximum. *Mar. Micropaleontol.*, **44**, 1–29.
- Fortuin, I. P. F., and J. Oerlemans, 1990: Parameterization of the annual surface temperature and mass balance of Antarctica. *Ann. Glaciol.*, **14**, 78–84.
- Gersonde, R., and G. Zielinski, 2000: The reconstruction of late Quaternary Antarctic sea-ice distribution—The use of diatoms as a proxy for sea-ice. *Palaeogeogr. Palaeoclimatol. Palaeoecol.*, **162**, 263–286.
- Graham, N. E., and T. P. Barnett, 1987: Sea surface temperature, surface wind divergence, and convection over tropical oceans. *Science*, **238**, 657–659.
- Guilderson, T. P., R. G. Fairbanks, and J. L. Rubenstone, 1994: Tropical temperature variations since 20,000 years ago: Modulating interhemispheric climate change. *Science*, **263**, 663–665.
- Hastings, D. W., A. D. Russell, and S. R. Emerson, 1998: Foraminiferal magnesium in *Globorinoides sacculifer* as a paleotemperature proxy. *Paleoceanography*, **13**, 161–169.
- Hebbeln, D., T. Dokken, E. S. Andersen, M. Hald, and A. Elverhøi, 1994: Moisture supply for northern ice-sheet growth during the Last Glacial Maximum. *Nature*, **370**, 357–360.
- Hewitt, C. D., A. J. Broccoli, J. F. B. Mitchell, and R. J. Stouffer, 2001a: A coupled model study of the Last Glacial Maximum: Was part of the North Atlantic relatively warm? *Geophys. Res. Lett.*, **28**, 1571–1574.
- , C. A. Senior, and J. F. B. Mitchell, 2001b: The impact of dynamic sea-ice on the climatology and climate sensitivity of a GCM: A study of past, present, and future climates. *Climate Dyn.*, **17**, 655–668.
- , R. J. Stouffer, A. J. Broccoli, J. F. B. Mitchell, and P. J. Valdes, 2003: The effect of ocean dynamics in a coupled GCM simulation of the Last Glacial Maximum. *Climate Dyn.*, **20**, 203–218.
- Hollin, J. T., and D. H. Schilling, 1981: Late Wisconsin–Weichselian

- mountain glaciers and small ice caps. *The Last Great Ice Sheets*, G. H. Denton and T. J. Hughes, Eds., Wiley, 179–220.
- Honda, M., K. Yamazaki, H. Nakamura, and K. Takeuchi, 1999: Dynamic and thermodynamic characteristics of atmospheric response to anomalous sea-ice extent in the Sea of Okhotsk. *J. Climate*, **12**, 3347–3358.
- Horel, J. D., and J. M. Wallace, 1981: Planetary-scale atmospheric phenomena associated with the Southern Oscillation. *Mon. Wea. Rev.*, **109**, 813–829.
- Hostetler, S. W., and A. C. Mix, 1999: Reassessment of ice-age cooling of the tropical ocean and atmosphere. *Nature*, **399**, 673–676.
- Hulton, N. R. J., R. S. Purves, R. D. McColloch, D. E. Sugden, and M. J. Bentley, 2002: The Last Glacial Maximum and deglaciation of southern South America. *Quat. Sci. Rev.*, **21**, 233–241.
- Kageyama, M., O. Peyron, S. Pinot, P. Tarasov, J. Guiot, S. Jousaume, and G. Ramstein, 2001: The Last Glacial Maximum climate over Europe and western Siberia: A PMIP comparison between models and data. *Climate Dyn.*, **17**, 23–43.
- Kiehl, J. T., J. J. Hack, G. B. Bonan, B. A. Boville, D. L. Williamson, and P. J. Rasch, 1998: The National Center for Atmospheric Research Community Climate Model: CCM3. *J. Climate*, **11**, 1131–1149.
- Lassen, S., E. Jansen, K. L. Knudsen, A. Kuijpers, M. Kristensen, and K. Christensen, 1999: Northeast Atlantic sea surface circulation during the past 30–10 ¹⁴C kyr B.P. *Paleoceanography*, **14**, 616–625.
- Lea, D. W., D. K. Pak, and H. J. Spero, 2000: Quaternary equatorial Pacific sea surface temperature variations. *Science*, **289**, 1719–1724.
- Lee, K. E., and N. C. Slowey, 1999: Cool surface waters of the subtropical North Pacific Ocean during the last glacial. *Nature*, **397**, 512–514.
- , N. C. Slowey, and T. D. Herbert, 2001: Glacial sea surface temperatures in the subtropical North Pacific: A comparison of U₃₇^k, δ¹⁸O, and foraminiferal assemblage temperature estimates. *Paleoceanography*, **16**, 268–279.
- Lindzen, R. S., and S. Nigam, 1987: On the role of sea surface temperature gradients in forcing low-level winds and convergence in the Tropics. *J. Atmos. Sci.*, **44**, 2418–2436.
- Lyle, M. W., F. G. Prahl, and M. A. Sparrow, 1992: Upwelling and productivity changes inferred from a temperature record in the central equatorial Pacific. *Nature*, **355**, 812–815.
- Manabe, S., and A. J. Broccoli, 1985: The influence of continental ice sheets on the climate of an ice age. *J. Geophys. Res.*, **90**, 2167–2190.
- Marsiat, I., and P. J. Valdes, 2001: Sensitivity of the Northern Hemisphere climate of the Last Glacial Maximum to sea surface temperatures. *Climate Dyn.*, **17**, 233–248.
- Miller, G. H., J. W. Magee, and A. J. T. Jull, 1997: Low-latitude glacial cooling in the Southern Hemisphere from amino-acid racemization in emu eggshells. *Nature*, **385**, 241–244.
- Mix, A. C., A. E. Morey, N. G. Pisias, and S. W. Hostetler, 1999: Foraminiferal faunal estimates of paleotemperature: Circumventing the no-analog problem yields cool ice age Tropics. *Paleoceanography*, **14**, 350–359.
- , E. Bard, and R. Schneider, 2001: Environmental processes of the ice age: Land, oceans, glaciers (EPILOG). *Quat. Sci. Rev.*, **20**, 627–657.
- Ohkouchi, N., K. Kawamura, T. Nakamura, and A. Taira, 1994: Small changes in the sea surface temperature during the last 20,000 years: Molecular evidence from the western tropical Pacific. *Geophys. Res. Lett.*, **21**, 2207–2210.
- Ortiz, J., A. Mix, S. Hostetler, and M. Kashgarian, 1997: The California Current of the last glacial maximum: Reconstruction at 42°N based on multiple proxies. *Paleoceanography*, **12**, 191–205.
- Peltier, W. R., 1994: Ice age paleotopography. *Science*, **265**, 195–201.
- Pisias, N. G., and A. C. Mix, 1997: Spatial and temporal oceanographic variability of the eastern equatorial Pacific during the late Pleistocene: Evidence from Radiolarian microfossils. *Paleoceanography*, **12**, 381–393.
- , A. Roelofs, and M. Weber, 1997: Radiolarian-based transfer functions for estimating mean surface temperature and seasonal range. *Paleoceanography*, **12**, 365–379.
- Prell, W. L., 1985: The stability of low-latitude sea-surface temperatures: An evaluation of the CLIMAP reconstruction with emphasis on the positive SST anomalies. U.S. Dept. of Energy Rep. DOE/ER/60167, 53 pp.
- Prentice, I. C., D. Jolly, and BIOME 6000 participants, 2000: Mid-Holocene and glacial-maximum vegetation geography of the northern continents and Africa. *J. Biogeogr.*, **27**, 507–519.
- Rasmusson, E. M., and J. M. Wallace, 1983: Meteorological aspects of the El Niño/Southern Oscillation. *Science*, **222**, 1195–1202.
- Rind, D., 1986: The dynamics of warm and cold climates. *J. Atmos. Sci.*, **43**, 3–24.
- , 1998: Latitudinal temperature gradients and climate change. *J. Geophys. Res.*, **103**, 5943–5971.
- , and D. Peteet, 1985: Terrestrial conditions at the Last Glacial Maximum and CLIMAP sea-surface temperature estimates: Are they consistent? *Quat. Res.*, **24**, 1–22.
- Ropelewski, C. F., and M. S. Halpert, 1989: Precipitation patterns associated with the high index phase of the Southern Oscillation. *J. Climate*, **2**, 268–284.
- Rosell-Melé, A., and N. Koç, 1997: Paleoclimatic significance of the stratigraphic occurrence of photosynthetic biomarker pigments in the Nordic seas. *Geology*, **25**, 49–52.
- , and P. Comes, 1999: Evidence for a warm Last Glacial Maximum in the Nordic seas or an example of shortcomings in U₃₇^k and U₃₇^h to estimate low sea surface temperature? *Paleoceanography*, **14**, 770–776.
- Ruddiman, W. F., and A. McIntyre, 1979: Warmth of the subpolar North Atlantic Ocean during Northern Hemisphere ice-sheet growth. *Science*, **204**, 173–175.
- Salamatin, A. N., V. Y. Lipenkov, N. I. Barkov, J. Jouzel, J. R. Petit, and D. Raynaud, 1998: Ice core age dating and temperature profiles from deep boreholes at Vostok Station (East Antarctica). *J. Geophys. Res.*, **103**, 8963–8977.
- Sarnthein, M., 1978: Sand deserts during glacial maximum and climatic optimum. *Nature*, **272**, 43–46.
- Shea, D. J., K. E. Trenberth, and R. W. Reynolds, 1992: A global monthly sea surface temperature climatology. *J. Climate*, **5**, 987–1001.
- Shin, S.-I., Z. Liu, B. Otto-Bliessner, E. C. Brady, J. E. Kutzbach, and S. P. Harrison, 2003: A simulation of the Last Glacial Maximum climate using the NCAR-CCSM. *Climate Dyn.*, **20**, 127–151.
- Sikes, E. L., and L. D. Keigwin, 1994: Equatorial Atlantic sea surface temperature for the last 30 kyr: A comparison of U₃₇^k, δ¹⁸O and foraminiferal assemblage temperature estimates. *Paleoceanography*, **9**, 31–45.
- Sonzogni, C., E. Bard, and F. Rostek, 1998: Tropical sea-surface temperatures during the last glacial period: A view based on alkenones in Indian Ocean sediments. *Quat. Sci. Rev.*, **17**, 1185–1201.
- Street, F. A., and A. T. Grove, 1979: Global maps of lake-level fluctuations since 30,000 years B.P. *Quat. Res.*, **12**, 83–118.
- Stute, M., P. Schlosser, J. F. Clark, and W. S. Broecker, 1992: Paleotemperatures in the southwestern United States derived from noble gases in ground water. *Science*, **256**, 1000–1003.
- , J. F. Clark, P. Schlosser, W. S. Broecker, and G. Bonani, 1995a: A 30,000 yr continental paleotemperature record derived from noble gases dissolved in groundwater from the San Juan Basin, New Mexico. *Quat. Res.*, **43**, 209–220.
- , M. Forster, H. Frischkorn, A. Serejo, J. F. Clark, P. Schlosser, W. S. Broecker, and G. Bonani, 1995b: Cooling of tropical Brazil (5°C) during the Last Glacial Maximum. *Science*, **269**, 379–383.
- Tarasov, P., and Coauthors, 1999: Last Glacial Maximum climate of the former Soviet Union and Mongolia reconstructed from pollen and plant microfossil data. *Climate Dyn.*, **15**, 227–240.

- Ternois, Y., M.-A. Sicre, and M. Paterne, 2000: Climatic changes along the northwestern African continental margin over the last 30 kyrs. *Geophys. Res. Lett.*, **27**, 133–136.
- Thompson, L. G., and Coauthors, 1998: A 25,000 year tropical climate history from Bolivian ice cores. *Science*, **282**, 1858–1864.
- , T. Yao, E. Mosley-Thompson, M. E. Davis, K. A. Henderson, and P.-N. Lin, 2000: A high-resolution millennial record of the South Asian monsoon from Himalayan ice cores. *Science*, **289**, 1916–1919.
- Trend-Staid, M., and W. L. Prell, 2002: Sea surface temperature at the Last Glacial Maximum: A reconstruction using the modern analog technique. *Paleoceanography*, **17**, 1065, doi:10.1029/2000PA000506.
- Veum, T., E. Jansen, M. Arnold, I. Beyer, and J.-C. Duplessy, 1992: Water mass exchange between the North Atlantic and the Norwegian Sea during the past 28,000 years. *Nature*, **356**, 783–785.
- Vincent, D. G., 1994: The South Pacific convergence zone (SPCZ): A review. *Mon. Wea. Rev.*, **122**, 1949–1970.
- Weaver, A. J., M. Eby, A. F. Fanning, and E. C. Wiebe, 1998: Simulated influence of carbon dioxide, orbital forcing and ice sheets on the climate of the Last Glacial Maximum. *Nature*, **394**, 847–853.
- Webster, P. J., 1972: Response of the tropical atmosphere to local, steady forcing. *Mon. Wea. Rev.*, **100**, 518–541.
- Weinelt, M., M. Sarnthein, U. Pflaumann, H. Schulz, S. Jung, and H. Erlenkeuser, 1996: Ice-free Nordic seas during the last glacial maximum? Potential sites of deepwater formation. *Paleoclimates*, **1**, 283–309.
- Weyhenmeyer, C. E., S. J. Burns, H. N. Waber, W. Aeschbach-Hertig, R. Kipfer, H. H. Loosli, and A. Matter, 2000: Cool glacial temperatures and changes in moisture source recorded in Oman groundwaters. *Science*, **287**, 842–845.
- Yin, J. H., and D. S. Battisti, 2001: The importance of tropical sea surface temperature patterns in simulations of Last Glacial Maximum climate. *J. Climate*, **14**, 565–581.
- Yokoyama, Y., K. Lambeck, P. De Deckker, P. Johnson, and K. Fifield, 2000: Timing of the Last Glacial Maximum from observed sea-level minima. *Nature*, **406**, 713–716.
- Zhang, C., 1993: Large-scale variability of atmospheric deep convection in relation to sea surface temperature in the Tropics. *J. Climate*, **6**, 1898–1913.